GEOPHYSICS, VOL. 71, NO. 2 (MARCH-APRIL 2006); P. Q9–Q17, 7 FIGS.
10.1190/1.2187777

A new elastic model for ground coupling of geophones with spikes

Guy G. Drijkoningen[1], Frederik Rademakers[1], Evert C. Slob[1], and Jacob T. Fokkema[1]

ABSTRACT

Ground coupling are terms that describe the transfer from seismic ground motion to the motion of a geophone. In previous models, ground coupling was mainly considered as a disk lying on top of a half-space, not considering the fact that in current practice geophones are spiked and are buried for optimal response. In this paper we introduce a new model that captures the spike added to the geophone and models the effect of geophone burial. The geophone is modeled as a rigid, movable cylinder embedded in a half-space near or at the surface. The coupling problem is then tackled by a scattering approach using the elastic form of reciprocity; we consider the vertical component only. The main feature in the coupling function is a resonance whose location and shape depend on the different parameters of the geophone and the soil. In accordance with previous models, adding mass reduces the frequency of resonance. However, we show that pure mass loading assumption is too restrictive for standard geophones. Our new model shows that increasing the spike radius and length decreases the frequency of resonance and the resonance is more peaked. Furthermore, burying the geophone decreases the frequency of resonance, but when one takes into account that the soil at depth is more compact, then the behavior is as observed in practice — namely, an increase in frequency of resonance. As for the properties of the soil, the shear-wave velocity has the largest effect; when increased, it shifts the frequency of resonance to the high-frequency end as desired.

INTRODUCTION

Accurate measurements of seismic motions in soil are often required in seismic exploration and earthquake studies as well as in mine blasting operations. Natural sources (e.g., earthquakes) or forced sources (e.g., dynamite) are the origin of this ground motion. Measuring devices are designed to produce an output that is linearly proportional to a quantity related to the ground motion in their immediate vicinity. In land seismic surveys for exploration and monitoring, geophones are used. They produce a voltage proportional to the particle velocity of the ground.

In practice, the transfer function from the particle velocity of the ground to the output voltage of the geophone is never constant. First, the geophone itself has a transfer function that generally dampens the signal below the resonance frequency of the coil. Second, the transfer of the seismic motion from the ground to the geophone, an exchange commonly called *geophone ground coupling*, is not perfect and therefore distorts the signal. Ground-coupling issues may play a prominent role in seismic exploration and monitoring when high-resolution seismic techniques are considered — the focus of this paper. In some cases, the frequencies of interest can exceed 1000 Hz. In the band above 100 Hz, the effect of the geophone coupling conditions is significant, as is shown in Krohn (1984) and Drijkoningen (2000) and as we discuss in this paper.

The ideal sensor measures ground motion (or a related quantity). One problem is that the presence of the measuring device itself disturbs the incoming wavefield, thus influencing the ground motion. A second problem is that the measured quantity is strongly influenced by the contact conditions between the device and the ground. When the spike is not in good contact with the earth, the coupling behavior is dominated by the mass of the geophone (via contact pressure) and can appropriately be called *weight coupling*.

In this paper, we focus on spike-shear coupling, which assumes the spike is in good contact with the soil and couples the geophone to the ground (Drijkoningen, 2000). In most publications on modeling geophone ground coupling, the geophone is modeled as a cylinder lying atop a half-space (Lamer, 1970; Hoover and O'Brien, 1980). While this is applicable for geophones in land streamers or lying on the seafloor, in most surveys the spike of the geophone furnishes the coupling between the geophone and the ground, and this must be taken into

Manuscript received by the Editor August 31, 2004; revised manuscript received July 4, 2005; published online March 9, 2006.
[1]Delft University of Technology, Applied Geophysics & Petrophysics, Mijnbouwstraat 120, 2628 RX Delft, The Netherlands, E-mail: g.g.drijkoningen@tudelft.nl; e.c.slob@tudelft.nl; j.t.fokkema@tudelft.nl.

account in modeling. Tan (1987) was the first author to do this. The quantitative effect for the acoustic approximation, not really valid for land seismics, is given by Vos et al. (1999).

A very general definition is used for ground coupling. When a wave arrives at the surface of the ground, the movement is represented by $\hat{v}^{\mathrm{gr}}(\omega)$ when no measuring device is present. When the geophone or measuring device is present, the movement is represented by $\hat{v}^{\mathrm{geo}}(\omega)$. The relationship between these two movements is the transfer function, called the coupling coefficient C:

$$C(\omega) = \frac{\hat{v}^{\mathrm{geo}}(\omega)}{\hat{v}^{\mathrm{gr}}(\omega)}. \tag{1}$$

When three components are measured, different components of the coupling can be considered. Thus, the coupling coefficient generally can be written as

$$C_{ij}(\omega) = \frac{\hat{v}_i^{\mathrm{geo}}(\omega)}{\hat{v}_j^{\mathrm{gr}}(\omega)}, \tag{2}$$

with $i, j \in \{1, 2, 3\}$; $\hat{v}_i^{\mathrm{geo}}(\omega)$ the ith component of the geophone, assuming a perfect geophone-ground contact, and $\hat{v}_j^{\mathrm{gr}}(\omega)$ the jth component of the velocity of the ground in the absence of the geophone. The cases for one-component geophones are the factors C_{ij} for $i = j$; this implies off-diagional terms are negligible.

Since the contact area of the geophone to the ground is mainly achieved by the spike, the geophone is modeled as a spike only. This differs from the model of a cylinder lying on the earth's surface used in previous studies (Lamer, 1970; Hoover and O'Brien, 1980).

Our discussion begins with basic equations describing wave motion; thereafter, the Green's functions are shown for free space and the elastic half-space. The latter is used in the elastic (Betti-Rayleigh) reciprocity theorem that gives a velocity boundary-integral equation for a scatterer in an elastic half-space. The discussion then investigates a rigid, cylindrical scatterer measuring the vertical wave motion as a model for a one-component vertical geophone. In the final expressions, only 1D integrations need be performed numerically. A particular item in these integrations is the presence of the Rayleigh pole, dealt with separately using Cauchy's theorem. Then, numerical results are shown for typical geophone configurations. The final section presents the conclusions.

BASIC ELASTIC EQUATIONS

To locate a point in space, Cartesian coordinates x, y, and z are used, which in this order form a right-handed system with the z-axis pointing downward into the earth. The state of a point in an elastic medium is described in the frequency domain by the particle velocity vector $\hat{v}_i(\mathbf{x}, \omega)$ and stress tensor $\hat{\tau}_{ij}(\mathbf{x}, \omega)$ at that particular point; we assume a time dependence of $\hat{f}(\omega)\exp(i\omega t)$ of all quantities, where the caret over a quantity denotes the frequency domain.

The basic equations describing wave motion are given by Newton's second law, the equation of motion:

$$-\partial_q \hat{\tau}_{qk} + i\omega\rho\hat{v}_k = \hat{f}_k, \tag{3}$$

in which ρ is the mass density and f_k is the volume source density of external forces. The deformation equation is

$$C_{ijpq}\partial_p \hat{v}_q - i\omega\hat{\tau}_{ij} = 0, \tag{4}$$

where no source term is assumed to be present and where elastic, isotropic, homogeneous media are assumed, i.e.,

$$C_{ijpq} = \lambda\delta_{ij}\delta_{pq} + \mu(\delta_{ip}\delta_{jq} + \delta_{iq}\delta_{jp}), \tag{5}$$

where λ and μ are the Lamé parameters.

FREE-SPACE GREEN'S FUNCTIONS

We want to quantify the scattering from the spike; therefore, the Green's functions for the free-space and half-space are needed. Let us first define $\hat{G}_P$ and $\hat{G}_S$, the free-space Green's functions for the P- and S-waves:

$$\{\hat{G}_P, \hat{G}_S\}(\mathbf{x}) = \frac{1}{4\pi|\mathbf{x}|}\{\exp(-i\omega|\mathbf{x}|/c_P), \exp(-i\omega|\mathbf{x}|/c_S)\} \quad \text{for } |\mathbf{x}| \neq 0, \tag{6}$$

where c_P and c_S are the wavespeeds of the P- and S-waves, respectively, i.e., $c_P = [(\lambda + 2\mu)/\rho]^{1/2}$ and $c_S = (\mu/\rho)^{1/2}$.

Then, the basic solution for the particle velocity from a point source is (de Hoop, 1995)

$$\hat{v}_r(\mathbf{x}, \omega) = i\omega\rho^{-1}\hat{f}_k(\omega)\hat{G}_{rk}(\mathbf{x}, \omega), \tag{7}$$

where

$$\hat{G}_{rk} = c_S^{-2}\hat{G}_S\delta_{rk} - \omega^{-2}\partial_r\partial_k(\hat{G}_P - \hat{G}_S). \tag{8}$$

Green's functions define a linear relationship between a point source and the wavefield quantities resulting from this point source; thus, they act as response functions. Expressing this leads to the following definition:

$$\{\hat{v}_p, \hat{\tau}_{pq}\}(\mathbf{x}|\mathbf{x}^R) = \hat{f}_k(\omega)\{\hat{\Gamma}_{pk}, \hat{G}_{pqk}\}(\mathbf{x}|\mathbf{x}^R). \tag{9}$$

Comparing this definition with equations 7 and 4, the Green's function for particle velocity $\hat{\Gamma}_{pk}$ and for stress $\hat{G}_{pqk}$ can be reconized as

$$\{\hat{\Gamma}_{pk}, \hat{G}_{pqk}\}(\mathbf{x}|\mathbf{x}^R) = \rho^{-1}\{i\omega\hat{G}_{pk}, C_{pqnr}\partial_n\hat{G}_{rk}\}(\mathbf{x}|\mathbf{x}^R). \tag{10}$$

HALF-SPACE GREEN'S FUNCTIONS

Referring to the definition for free space (equation 9), a similar definition for the half-space Green's functions is introduced:

$$\{\hat{v}_p^H, \hat{\tau}_{pq}^H\}(\mathbf{x}|\mathbf{x}^R) = \hat{f}_k(\omega)\{\hat{\Gamma}_{pk}^H, \hat{G}_{pqk}^H\}(\mathbf{x}|\mathbf{x}^R). \tag{11}$$

The superscript H indicates these Green's functions apply to a half space.

The next logical step, as in the acoustic case, would be to express Green's functions for the half-space in terms of Green's functions for free space. However, in the elastic case we must decompose the wavefield into its different components, P- and S-waves. This is a problem solved for a half-space [see, for example, Aki and Richards (1980) and de Hoop and Van der Hijden (1985)]. The relevant expressions are given in Appendix A. However, since the expressions are derived in the

spatial Fourier-transformed domain, an inverse transformation must be performed.

CONTRASTING DOMAIN IN HALF-SPACE

A cylindrical spike planted vertically at the earth's surface obviously may be considered a scattering subdomain, where the scatterer is embedded in a background solid. The object of bounded support D_{scat} has known elastodynamic properties differing from those of the embedding material. The scatterer is elastodynamically irradiated by the given surface sources on $\partial D_{\text{source}}$, located outside the scattering domain. The resulting wavefield can be decomposed into two wavefields;

1) the incident wavefield, i.e., the wavefield that would exist in the entire configuration if the object showed no contrast with respect to its embedding material or the half-space wavefield;
2) the scattered wavefield, i.e., the wavefield resulting from an equivalent contrast surface source distribution located on ∂D_{scat}. This represents the mathematical image of the reflection of the incident waves at the scattering surface.

Because of the linearity of the basic elastodynamic equations, the total wavefield is the sum of the incident wavefield and the scattered wavefield. For the particle velocities and the dynamic stresses, these are expressed by, respectively,

$$\hat{v}_k^{\text{tot}}(\mathbf{x}) = \hat{v}_k^H(\mathbf{x}) + \hat{v}_k^{\text{scat}}(\mathbf{x}) \tag{12}$$

and

$$\hat{\tau}_{pq}^{\text{tot}}(\mathbf{x}) = \hat{\tau}_{pq}^H(\mathbf{x}) + \hat{\tau}_{pq}^{\text{scat}}(\mathbf{x}). \tag{13}$$

We assume that the geophone at the point of observation $\mathbf{x}^R$ is situated on the scattering surface. The incident field may then be written

$$-\int_{\mathbf{x}\in\partial D_{\text{scat}}} \left[\hat{G}_{pqk}^H(\mathbf{x}|\mathbf{x}^R)\hat{v}_p^H(\mathbf{x}) - \hat{\Gamma}_{pk}^H(\mathbf{x}|\mathbf{x}^R)\hat{\tau}_{pq}^H(\mathbf{x})\right]\nu_q dA = \frac{1}{2}\hat{v}_k^H(\mathbf{x}^R) \quad \text{when } \mathbf{x}^R \in \partial D_{\text{scat}}. \tag{14}$$

The scattered wavefield may then be written

$$\int_{\mathbf{x}\in\partial D_{\text{scat}}} \left[\hat{G}_{pqk}^H(\mathbf{x}|\mathbf{x}^R)\hat{v}_p^{\text{scat}}(\mathbf{x}) - \hat{\Gamma}_{pk}^H(\mathbf{x}|\mathbf{x}^R)\hat{\tau}_{pq}^{\text{scat}}(\mathbf{x})\right]\nu_q dA = \frac{1}{2}\hat{v}_k^{\text{scat}}(\mathbf{x}^R) \quad \text{when } \mathbf{x}^R \in \partial D_{\text{scat}}. \tag{15}$$

Subtracting equations 14 from 15 results in

$$\int_{\mathbf{x}\in\partial D_{\text{scat}}} \left[\hat{G}_{pqk}^H(\mathbf{x}|\mathbf{x}^R)\hat{v}_p^{\text{tot}}(\mathbf{x}) - \hat{\Gamma}_{pk}^H(\mathbf{x}|\mathbf{x}^R)\hat{\tau}_{pq}^{\text{tot}}(\mathbf{x})\right]\nu_q dA = \frac{1}{2}\hat{v}_k^{\text{tot}}(\mathbf{x}^R) - \hat{v}_k^H(\mathbf{x}^R) \quad \text{when } \mathbf{x}^R \in \partial D_{\text{scat}}. \tag{16}$$

COUPLING COEFFICIENT FOR RIGID MOVABLE CYLINDER

The role of the scatterer is played by the geophone spike because in practical situations it is much more rigid than its surroundings. In modeling, we assume this object is perfectly rigid. This permits the assumption of a constant particle velocity within the object equal to $\hat{V}_p^{\text{tot}}$. The object is then movable. In the model, the contact between the spike and the ground is assumed to be firm. The consequence of this is a constant velocity of the ground particles along the object's surface. To satisfy the requirement of finding a relationship between the geophone motion and the motion of the ground with no geophone present, equation 16 is needed. Since $\hat{V}_p^{\text{tot}}$ is constant, it can be taken outside the integral. Equation 16 then becomes

$$\frac{1}{2}\hat{V}_k^{\text{tot}}(\mathbf{x}^R) = \hat{v}_k^H(\mathbf{x}^R) + \hat{V}_p^{\text{tot}}(\mathbf{x}^R) \times \int_{\mathbf{x}\in\partial D_{\text{scat}}} \hat{G}_{pqk}^H(\mathbf{x}|\mathbf{x}^R)\nu_q dA - \int_{\mathbf{x}\in\partial D_{\text{scat}}} \hat{\Gamma}_{pk}^H(\mathbf{x}|\mathbf{x}^R)\hat{\tau}_{pq}^{\text{tot}}(\mathbf{x})\nu_q dA. \tag{17}$$

In the other integral with $\hat{\tau}_{pq}^{\text{tot}}$, none of the terms is constant. To place the term $\hat{\tau}_{pq}^{\text{tot}}$ outside the integral, which is necessary if we are to define a coupling coefficient, the equation of motion for the geophone itself must be solved by directly integrating the equation of motion 3 over the volume occupied by the geophone spike, i.e.,

$$\int_{\mathbf{x}\in\partial D} \hat{\tau}_{pq}\nu_q dA = i\omega\hat{V}_p \int_{\mathbf{x}\in D} \rho_{\text{geo}} dV, \tag{18}$$

in which ρ_{geo} is the density of the geophone spike.

We can now assume that a solution exists for the stress as a function of the spatially constant velocity $\hat{V}_3$:

$$\hat{\tau}_{33} = i\omega\rho_{\text{geo}} z \hat{V}_3^{\text{tot}}, \tag{19}$$

$$\hat{\tau}_{pq} = 0 \quad \text{for} \quad \{p,q\} \neq \{3,3\}. \tag{20}$$

These are strong assumptions, and this is not a unique solution. That this is one solution can be seen by substituting it in equation 18 and applying Gauss' divergence theorem. These assumptions require that we consider vertical motion of the geophone only as the vertical component of P- or S-waves.

Here, we introduce the geometry of a cylindrical spike. The definition of the sizes of the cylinder and the coordinate axes are depicted in Figure 1. The scattering surface ∂D_{scat} of the cylinder is divided into three parts: a top (∂D_{top}), a mantle (∂D_{man}), and a bottom (∂D_{bot}).

Now let us return to the solution for the stress (equations 19 and 20) and the last integral in equation 17 for the vertical component ($k = 3$). At the mantle of the cylinder, the vertical component of the normal to the cylinder is zero. At the top and bottom they are not zero, but there the stress is constant according to equation 19. As a result, the total field for the vertical component becomes

$$\frac{1}{2}\hat{V}_3^{\text{tot}}(\mathbf{x}^R) = \hat{v}_3^H(\mathbf{x}^R) + \hat{V}_3^{\text{tot}}(\mathbf{x}^R) \times \left[\int_{\mathbf{x}\in\partial D_{\text{scat}}} \hat{G}_{3q3}^H(\mathbf{x}|\mathbf{x}^R)\nu_q dA + i\omega\rho_{\text{geo}}h_1 \times \int_{\mathbf{x}\in\partial D_{\text{top}}} \hat{\Gamma}_{33}^H(\mathbf{x}|\mathbf{x}^R)dA - i\omega\rho_{\text{geo}}h_2 \int_{\mathbf{x}\in\partial D_{\text{bot}}} \hat{\Gamma}_{33}^H(\mathbf{x}|\mathbf{x}^R)dA\right], \tag{21}$$

where h_1 and h_2 are the depths of the top and bottom of the cylinder (see Figure 1), respectively, and we take into account that the normals ν_3 are in opposite directions. In this expression, a mass-loading term can be recognized: In the case that the top of the cylinder is at the surface ($h_1 = 0$), the term $\rho_{\text{geo}} h_2$ can be written as $M/(\pi R^2)$, where M is mass and R is the radius of the cylinder. So, if needed, an extra mass loading can be included here (in accordance with Hoover and O'Brien, 1980).

We now need to obtain a coupling coefficient, as defined in the introduction, where the wavefield without the geophone is the half-space field. The coupling coefficient for the vertical component can thus be defined as

$$C = \frac{\hat{V}_3^{\text{tot}}}{\hat{v}_3^H}. \tag{22}$$

Let us also split the first integral occurring in equation 21 into contributions of the top, mantle, and bottom of the cylinder. At the top and bottom of the cylinder, the horizontal components of the normal are zero (and if the top is at the surface, the Green's function $\hat{G}^H_{3q3}$ vanishes because the surface is stress free). At the mantle of the cylinder, the vertical component of the normal to the cylinder is zero. So the first integral in equation 21 becomes

$$\begin{aligned}
&\int_{\mathbf{x}\in\partial D_{\text{scat}}} \hat{G}^H_{3q3}(\mathbf{x}|\mathbf{x}^R)\nu_q\, dA \\
&= \int_{\mathbf{x}\in\partial D_{\text{man}}} \left[\hat{G}^H_{313}(\mathbf{x}|\mathbf{x}^R)\nu_1 + \hat{G}^H_{323}(\mathbf{x}|\mathbf{x}^R)\nu_2\right] dA \\
&\quad + \int_{\mathbf{x}\in\partial D_{\text{bot}}} \hat{G}^H_{333}(\mathbf{x}|\mathbf{x}^R) dA \\
&\quad - \int_{\mathbf{x}\in\partial D_{\text{top}}} \hat{G}^H_{333}(\mathbf{x}|\mathbf{x}^R) dA.
\end{aligned} \tag{23}$$

Thus far, the expressions for the Green's functions of the half-space have been general but still need to be specified. These can be found in Appendix B. The final expressions for a cylinder are such that the dominant terms are evaluated analytically. The integral over the mantle of the cylinder is

$$\begin{aligned}
&\int_{\mathbf{x}\in\partial D_{\text{man}}} \left[\hat{G}^H_{313}(\mathbf{x}|\mathbf{x}^R)\nu_1 + \hat{G}^H_{323}(\mathbf{x}|\mathbf{x}^R)\nu_2\right] dA \\
&= -\frac{1}{2} - i\omega^2 R \\
&\quad \times \int_{p=0}^{\infty} \left[\int_{z=h_1}^{h_2} \tilde{g}^H_1(p,z)dz - \frac{1}{2i\omega p}\right] p J_1(\omega p R) dp,
\end{aligned} \tag{24}$$

where J_1 denotes the first-order Bessel function and $\tilde{g}^H_1(p,z)$ is given in Appendix B. The integral over z can be performed analytically.

The integrals over the bottom of the cylinder are

$$\begin{aligned}
&\int_{\mathbf{x}\in\partial D_{\text{bot}}} \hat{G}^H_{333}(\mathbf{x}|\mathbf{x}^R) dA \\
&\quad = \frac{1}{2} + \omega R \int_{p=0}^{\infty} \tilde{g}^H_3(p, z = h_2) J_1(\omega p R) dp,
\end{aligned} \tag{25}$$

where $\tilde{g}^H_3(p,z)$ is given in Appendix B and use is made of some characteristics of the Bessel functions. In addition,

$$\begin{aligned}
&\int_{\mathbf{x}\in\partial D_{\text{bot}}} \hat{\Gamma}^H_{33}(\mathbf{x}|\mathbf{x}^R) dA \\
&\quad = \omega R \int_{p=0}^{\infty} \tilde{\gamma}^H_3(p, z = h_2) J_1(\omega p R) dp,
\end{aligned} \tag{26}$$

where $\tilde{\gamma}^H_3(p,z)$ is also given in Appendix B. The integrals over the top of the cylinder are equal to the bottom, but with $z = h_1$, and in equation 25, the factor $1/2$ is not removed from the integrand. The last integral in equation 26 for depth h_2 being zero is equivalent to the integral in Hoover and O'Brien (1980, their formula 13).

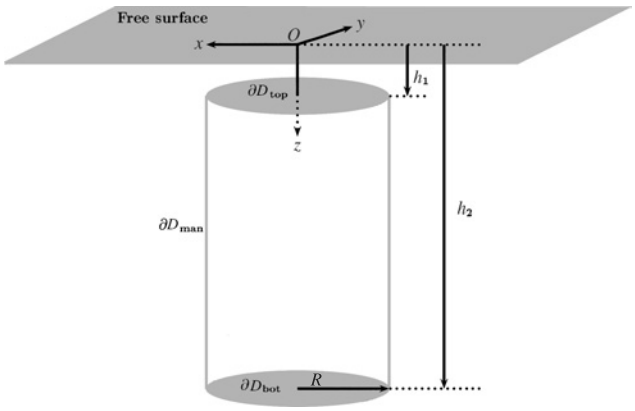

Figure 1. Configuration of a buried cylindrical contrast.

NUMERICAL IMPLEMENTATION

In the final expressions, each integral contains a pole so the pole contributions must be treated carefully using Cauchy's residue theorem. The integrand can be written generally as a function $f(p)/R(p)$, where the function $f(p)$ is the regular part of the integral and $R(p)$ is the function describing the pole, known as the Rayleigh pole. Applying Cauchy's residue theorem then leads to

$$\begin{aligned}
\int_0^{\infty} \frac{f(p)}{R(p)} dp &= \int_0^{\infty} \frac{f(p)R'(p_R)(p^2 - p_R^2) - 2p_R f(p_R)R(p)}{R(p)R'(p_R)(p^2 - p_R^2)} dp \\
&\quad + \pi j \frac{f(p_R)}{R'(p_R)}.
\end{aligned} \tag{27}$$

The branch points at the slownesses of the P- and S-waves must be treated carefully, since there the integral has (integrable) singularities. This has been treated by dividing the integral into pieces, with the branch points serving as end points for each subinterval and then integrating those using a Gaussian quadrature method.

NUMERICAL RESULTS

We now show some numerical results — in particular, the dependence of the coupling on the model's parameters. The results pertain to vertical components only, being the vertical component of P- or S-waves. There are two types of results:

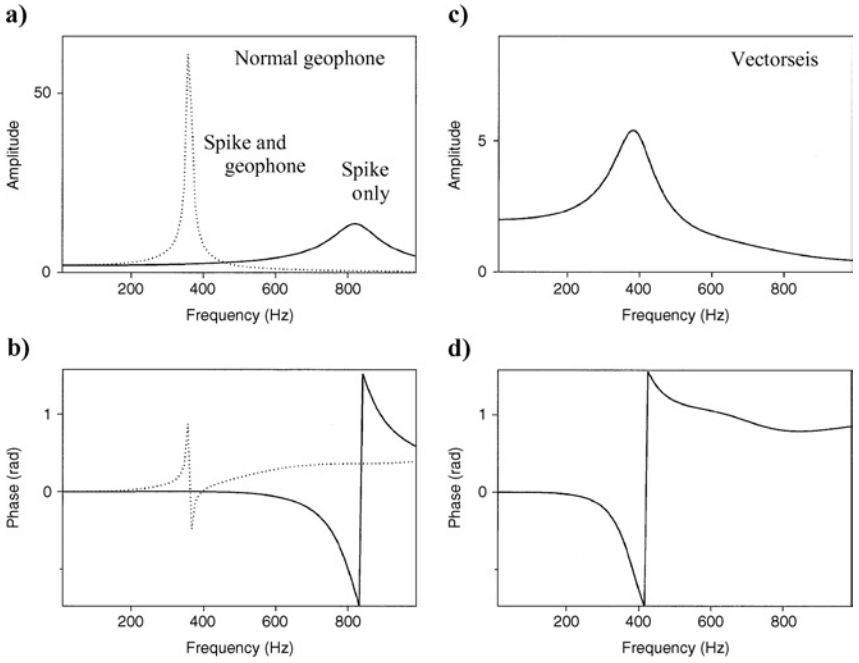

Figure 2. Coupling coefficient C for different configurations at the surface ($h_1 = 0$). Reference soil properties: $c_P = 200$ m/s, $c_S = 105$ m/s, and $\rho = 2$ g/cm^3. (a) Amplitude with cylinder representing spike only (solid line, $h_2 = 10$ cm, $R = 0.5$ cm, $\rho_{\text{geo}} = 2.653$ g/cm^3, equivalent mass = 20.84 g) and effective spike, representing spike and geophone (dotted line, $h_2 = 13.3$ cm, $R = 1.12$ cm, $\rho_{\text{geo}} = 5.044$ g/cm^3, equivalent mass = 265 g). (b) Phase of configurations of (a). (c) Amplitude of Vectorseis element ($h_2 = 15.5$ cm, $R = 2.5$ cm, $\rho_{\text{geo}} = 1.479$ g/cm^3, equivalent mass = 450 g). (d) Phase of configuration of (c).

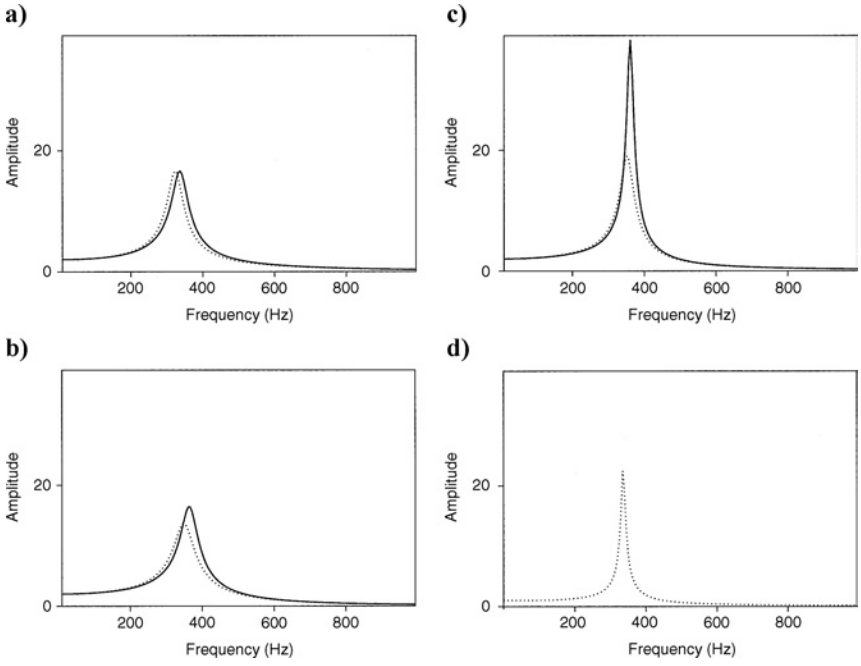

Figure 3. Contributions of mass-loading term in coupling coefficient C for constant mass and radius. Soil parameters are as for Figure 2; mass = 265 g, $R = 1.12$ cm, and $h_1 = 0$. Solid line is based on full expressions; dotted line is based on mass-loading term only. (a) $h_2 = 0.04$ cm and $\rho_{\text{geo}} = 16.771$ g/cm^3 (b) $h_2 = 0.08$ cm and $\rho_{\text{geo}} = 8.386$ g/cm^3, (c) $h_2 = 0.12$ cm and $\rho_{\text{geo}} = 5.590$ g/cm^3. (d) According to Hoover and O'Brien (1980) model.

those deriving from design aspects (shapes and sizes of geophones/spikes) and those obtained from the effects of field use. For design aspects, a certain range of expected soil parameters is engaged and firmly fixed, and the geophone parameters are then varied. For field effects, it is important to know the effect of coupling as a function of frequency, because it is possible to change only the burial depth of the geophone and not the parameters of the soil.

Some standard configurations are considered first (see Figure 2). In the first case (Figures 2a, 2b) the cylinder is modeled to represent the spike only (solid curves) and to represent the spike and the geophone, including the mass-coil system with its housing (dotted curves). For the latter case, an effective spike has been taken whose mass and volume equal those of a normal geophone. The coupling coefficient becomes two when approaching frequency zero. This results from the factor $1/2$ on the left-hand side in equation 21, which occurs because of measurement on the scattering surface. Note that the amplitude of the coupling function shows a maximum, associated with a resonance in the system that is observable in both the amplitude and the phase behavior. This is expected because a coupling frequency exists for anything that is placed on or in the ground. When looking at the two different cases, we can see that the effective spike, being thicker and heavier, reduces the frequency of resonance and the resonance is more peaked. In the second case, (Figures 2c, 2d) we model the cylinder representing the Vectorseis elements from Input/Output Inc., which has a different shape than standard geophones and is significantly larger. The resonance is relatively broad. For the purposes intended, i.e., frequencies 1–200 Hz, its size hardly affects the total reponse. However, when it is used for high-resolution surveying, coupling effects need to be considered seriously.

In Figure 3 the different contributions to the coupling are shown, specifically focused on the effect of mass loading. Physically, the case of mass loading on the surface is different from embedding a spike in the ground. Pure mass loading introduces a sag of the ground which has its own eigenfrequency. In the case of an embedded spike, this is not the only phenomenon. This means that the full expressions as in equation 21 are compared by taking only the mass-loading term in square brackets in that equation, i.e., only $\hat{\Gamma}^H_{33}$ (and h_1 being zero). Figure 3 shows how important

mass loading is, compared with the other terms. To that end, the length and density of the cylinder are changed, but both the mass and the radius of the cylinder are kept constant with the parameters of the effective spike. When the length of the spike is 4 cm as in Figure 3a, mass loading gives the main contribution to the coupling. However, when the length of the spike increases (and the density decreases to keep the mass constant), the contribution of mass loading is reduced, as seen in Figures 3b and 3c. For completeness, the response calculated from the model of Hoover and O'Brien (1980) is given in Figure 3d; this model assumes a pure mass loading. We can observe that this model compares well with only the mass-loading term in our new model. A difference exists in that the response from the model of Hoover and O'Brien is slightly more peaked than our mass-loading term.

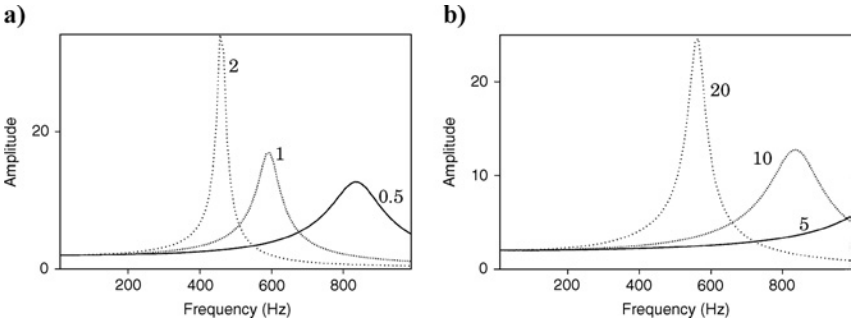

Figure 4. Effect of spike dimensions (radius and length) on amplitude of coupling coefficient C . Parameters are as for the cylinder representing the spike only, with the top at the surface $h_1 = 0$ (Figure 2a) apart from (a) radius R of cylinder is 0.5 cm (solid curve), 1 cm (finely dotted curve), and 2 cm (coarsely dotted curve). (b) Length of cylinder is 5 cm (solid curve), 10 cm (finely dotted curve), and 20 cm (coarsely dotted curve).

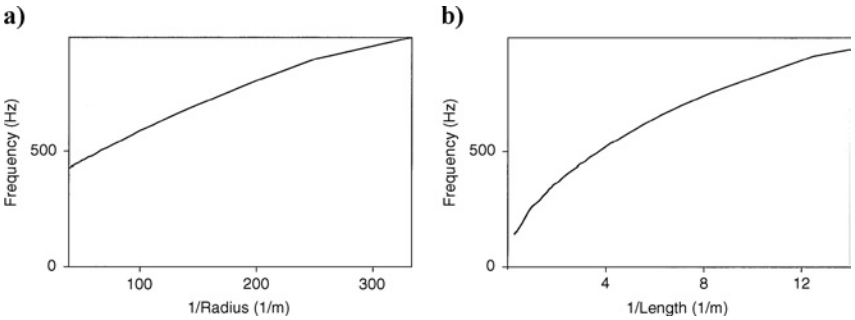

Figure 5. Effect of dimensions (1/radius and 1/length) of spike on frequency for maximum of coupling function C. Density of spike and parameters for soil are as for the cylinder representing the spike only, with the top at the surface as in Figure 2a.

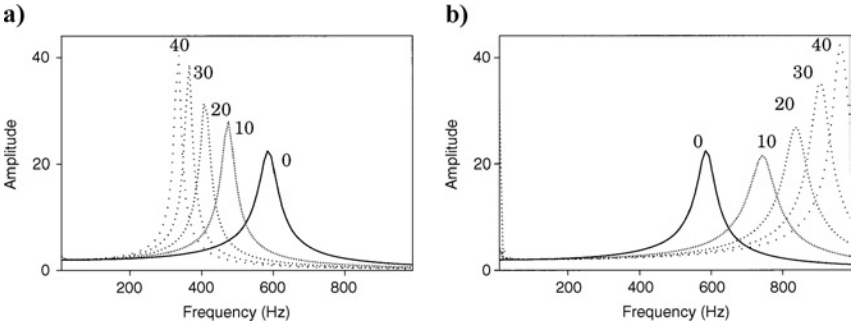

Figure 6. Effect of cylinder burial on amplitude of coupling coefficient C. Parameters are the same as for the cylinder representing the spike only (Figure 2a) apart from the length of the spike $(h_2 - h_1)$ being 20 cm. (a) Value c_S is constantly 105 m/s, and depth h_1 is 0 cm (solid curve), 10 cm (finely dotted curve), 20 cm (dotted curve), 30 cm (coarsely dotted curve), and 40 cm (very coarsely dotted curve); (b) c_S and depth h_1 both increase $c_S = 105$ m/s and $h_1 = 0$ cm (solid curve), $c_S = 150$ m/s and $h_1 = 10$ cm (finely dotted curve), $c_S = 200$ m/s and $h_1 = 20$ cm (coarsely dotted curve), $c_S = 250$ m/s and $h_1 = 30$ cm (coarsely dotted curve), and $c_S = 300$ m/s and $h_1 = 40$ cm (very coarsely dotted curve).

The next figures reflect varied parameters for the new model. For the first set, the parameters of the geophone are varied while keeping the parameters of the soil fixed. In Figure 4a, the radius of the spike is varied. The resonance shifts to lower frequencies and sharpens when the radius increases. The same can be observed for the length of the spike in Figure 4b: When the length increases, the resonance shifts to lower frequencies and sharpens. From Figure 4b it is unclear how this shift occurs. Therefore, in Figure 5 the resonance frequency is set out as a function of the inverse of radius and length. This shows a monotonically increasing trend; for the inverse of the radius, it is nearly linear.

In the second set of figures, the parameters for field use are varied, i.e., burial depth and soil parameters. First, we consider the effect of burial depth, as shown in Figure 6. We know from field experience that coupling improves significantly when a geophone is buried (Krohn, 1984). Therefore, first we model the effect of burying where we only increase burial depth. This result, shown in Figure 6a, is the opposite of field observations. However, we assume the properties of the soil do not change with depth, while in the field the soil is (sometimes much) more compacted at some depth than at the surface. Shearwave velocities can be well below 100 m/s in the first few centimeters from the surface while reaching a few hundred meters per second at some decimeters' depth. In swamp areas, spikes of more than 1 m have been used to reach more compacted ground. Therefore, we change both the burial depth of the geophone and the shear-wave velocity of the soil simultaneously (Figure 6b). The coupling improves because the resonance frequency becomes higher, which is now purely an effect of improved soil conditions at depth.

Next, the soil parameters are varied while keeping the geophone parameters fixed. In Figure 7a the P-wave speed is varied from values for a dry air-filled soil

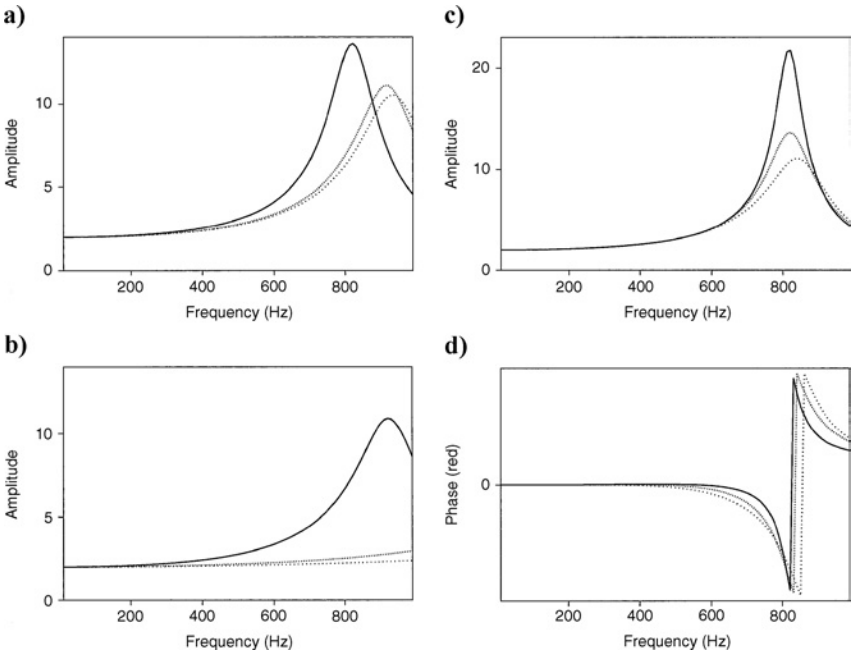

Figure 7. Effect of soil parameters are on coupling coefficient C. Parameters are the same as for a cylinder representing the spike only (Figure 2a) apart from (a) c_P being 200 m/s (solid curve), 500 m/s (finely dotted curve), and 1500 m/s (coarsely dotted curve); (b) c_P being 600 m/s and c_S being 105 m/s (solid curve), 200 m/s (finely dotted curve), and 300 m/s (coarsely dotted curve); (c) Lamé parameters λ and μ being 3.59×10^7 and 2.205×10^7, respectively, and ρ being 1.5 g/cm^3 (solid curve), 2 g/cm^3 (finely dotted curve), and 2.653 g/cm^3, which is the same as spike density (coarsely dotted curve); (d) phase of (c).

(200 m/s) to values for a fully water-saturated soil (1500 m/s). The P-wave speed does not have a big influence on coupling; little change takes place, although the P-wave speed changes dramatically (from 200–1500 m/s). Of great importance is the S-wave speed of the soil, as seen in Figure 7b: The higher the S-wave speed, the better the coupling. Resonance takes place above 1000 Hz. This can be explained by the integral over the mantle, which is proportional to the shear-wave velocity of the soil. Finally, Figures 7c and 7d show the dependence on soil density. Here, the parameters are changed such that the Lamé parameters remain constant but not the velocities, since the velocities still depend on the density (see beyond equation 8). The density variation has an influence on the amplitude of the coupling, not on the location and the broadness (see Figure 7d) of the resonance frequency; the frequency at which resonance occurs remains nearly the same. Tan (1984) notes that the density of the spike should match the density of the soil, but this is not sufficient to maintain a constant coupling, as shown by the coarsely dotted curve in Figure 7c, where the density of the soil is taken as equal to the density of the spike.

CONCLUSIONS

We introduce a new model for geophone-ground coupling that agrees better with seismic practice than previous models. The new model is a good representation for spike-shear coupling, while the previous models are more representative of pure weight coupling. The geophone is considered as consisting only of a spike, which is assumed to be perfectly rigid and in good physical contact with the soil (a slip-free model). The new model now predicts the behavior of a spike, common in seismic exploration and monitoring. Both mass loading and embedding are determined in its response. Further, the frequency of resonance in the coupling function is inversely proportional to the radius and length of the spike. Our new model allows us to predict the behavior of burying the geophone at depth. Although for a homogeneous half-space the resonance shifts to lower frequencies when we bury the geophone deeper, this effect is reversed when the shear-wave velocity is increased with depth as well. A shift of resonance to higher frequencies that occurs from burying the geophone is often seen in practice. With respect to soil parameters, P-wave velocity has little effect on coupling, while the effect of S-wave velocity is much more pronounced. Density variations change the amplitude of the coupling only, and the coupling still shows a resonance when the density of the spike matches the density of the soil.

APPENDIX A

REFLECTION COEFFICIENTS AT A STRESS-FREE INTERFACE

In the determination of the final expressions given in the main text, the reflection coefficients at a stress-free surface — i.e., the earth's surface — are needed. Here they are defined and given in the spatial Fourier domain. For the horizontal directions, the forward Fourier transform is defined as

$$\tilde{G}(p_1, p_2) = \int_{-\infty}^{+\infty}\int_{-\infty}^{+\infty} \hat{G}(x, y) \times \exp(+i\omega p_1 x + i\omega p_2 y)dxdy. \quad \text{(A-1)}$$

where $\omega > 0$. Incorporating this transform into the basic equations, the incident field for particle displacement $\mathbf{u}^{\text{inc}}$ can be found. When the source is located at $(0, 0, z^s)$, it is given as

$$\begin{pmatrix} \tilde{u}_1^{\text{inc}} \\ \tilde{u}_2^{\text{inc}} \\ \tilde{u}_3^{\text{inc}} \end{pmatrix} = \begin{pmatrix} p_1 \\ p_2 \\ -q_P \end{pmatrix} \tilde{A}_P^{\text{inc}} \exp[i\omega q_P(z - z^s)] + \begin{pmatrix} \frac{q_S p_1}{p} \\ \frac{q_S p_2}{p} \\ p \end{pmatrix} \tilde{A}_{SV}^{\text{inc}} \exp[i\omega q_S(z - z^s)] + \begin{pmatrix} p_2 \\ -p_1 \\ 0 \end{pmatrix} \tilde{A}_{SH}^{\text{inc}} \exp[i\omega q_S(z - z^s)] \quad (z < z^s), \quad \text{(A-2)}$$

where p stands for $p = (p_1^2 + p_2^2)^{1/2}$ and $q_{P,S} = (1/c_{P,S}^2 - p^2)^{1/2}$, with $\mathrm{Im}\{q_{P,S}\} < 0$. The amplitudes of the different wavefield constituents are determined by the nature of the source, $\tilde{f}_k(\omega)$ herein, and are functions of p_1, p_2, z, and ω. The total incident wavefield consists of three wave constituents: P-, SV-, and SH-waves.

For the reflected wavefield,

$$\begin{aligned}\begin{pmatrix}\tilde{u}_1^{\mathrm{refl}}\\ \tilde{u}_2^{\mathrm{refl}}\\ \tilde{u}_3^{\mathrm{refl}}\end{pmatrix} = &\begin{pmatrix}p_1\\ p_2\\ q_P\end{pmatrix}\left[\tilde{R}_{PP}\tilde{A}_P^{\mathrm{inc}}\exp(-i\omega q_P z^s)\right.\\ &\left.+\tilde{R}_{PS}\tilde{A}_{SV}^{\mathrm{inc}}\exp(-i\omega q_S z^s)\right]\exp(-i\omega q_P z)\\ &+\begin{pmatrix}\frac{q_S p_1}{p}\\ \frac{q_S p_2}{p}\\ -p\end{pmatrix}\left[\tilde{R}_{SP}\tilde{A}_P^{\mathrm{inc}}\exp(-i\omega q_P z^s)\right.\\ &\left.+\tilde{R}_{SS}\tilde{A}_{SV}^{\mathrm{inc}}\exp(-i\omega q_S z^s)\right]\exp(-i\omega q_S z)\\ &+\begin{pmatrix}p_2\\ -p_1\\ 0\end{pmatrix}\tilde{A}_{SH}^{\mathrm{inc}}\exp[-i\omega q_S(z+z^s)], \quad \text{(A-3)}\end{aligned}$$

which now includes the reflection coefficients at the stress-free surface yet to be determined.

The total wavefield of the half-space is the sum of the incident and the reflected wavefields, or

$$\tilde{u}_r^H = \tilde{u}_r^{\mathrm{inc}} + \tilde{u}_r^{\mathrm{refl}}. \quad \text{(A-4)}$$

For an incident P-wave, the different stress components can be written as a function of $\tilde{A}_P^{\mathrm{inc}}$. The same can be done for an incident SV-wave with $\tilde{A}_{SV}^{\mathrm{inc}}$. The boundary conditions at a stress-free interface are such that all components of the surface traction vanish — for this case, in the horizontal plane $z = 0$, i.e.,

$$\tilde{\tau}_{i3}^H = 0 \quad \text{for} \quad i = 1, 2, 3 \quad \text{at} \quad z = 0. \quad \text{(A-5)}$$

Implementing these boundary conditions results in the expressions for the reflection coefficients:

$$\tilde{R}_{PP} = -\tilde{R}_{SS} = \frac{4p^2 q_P q_S - \left(\frac{1}{c_S^2} - 2p^2\right)^2}{4p^2 q_P q_S + \left(\frac{1}{c_S^2} - 2p^2\right)^2} \quad \text{(A-6)}$$

$$\tilde{R}_{PS} = \frac{4pq_S\left(\frac{1}{c_S^2} - 2p^2\right)}{4p^2 q_P q_S + \left(\frac{1}{c_S^2} - 2p^2\right)^2}, \quad \text{(A-7)}$$

$$\tilde{R}_{SP} = \frac{4pq_P\left(\frac{1}{c_S^2} - 2p^2\right)}{4p^2 q_P q_S + \left(\frac{1}{c_S^2} - 2p^2\right)^2}. \quad \text{(A-8)}$$

APPENDIX B

HALF-SPACE GREEN'S FUNCTIONS

In this appendix, the expressions for the half-space Green's functions, i.e., $\tilde{G}_{pqk}^H$ and $\tilde{\Gamma}_{pk}^H$, are given. Only those expressions that occur in coupling vertical geophones are used, as defined in the main text.

The procedure is as follows: First, a spatial Fourier transform of the equations governing wave motion is applied. Next, the total field of the half-space is determined using an incident-field part and a reflected-field part. In the expressions of the incident and reflected fields, the amplitude coefficients A_P^{inc}, A_{SV}^{inc}, and A_{SH}^{inc} are still unknown and must be determined in terms of the forces f_i. By substituting these expressions in the total field of the half-space, the Green's functions can be determined.

In Appendix A, the spatial Fourier transform is defined. The total incident wavefield for the particle displacement can be written as

$$\tilde{u}_r^{\mathrm{inc}} = \tilde{U}_{rk}\tilde{A}_k^{\mathrm{inc}}. \quad \text{(B-1)}$$

In the main text, the solution for the free space in the $(\mathbf{x}, \omega)$ domain is determined, but here its representation in the horizontal-slowness domain is needed:

$$\tilde{u}_r^{\mathrm{inc}}(p_1, p_2, z, \omega) = \rho^{-1}\tilde{G}_{rk}(p_1, p_2, z - z^s, \omega)\tilde{f}_k(\omega), \quad \text{(B-2)}$$

in which the Green's functions $\tilde{G}_{rk}$ are the (p_1, p_2, z, ω)-domain expressions of equation 7 in the main text. This equation can be combined with equation B-1 to obtain

$$\tilde{A}_k^{\mathrm{inc}} = \rho^{-1}(\tilde{U}^{-1})_{rk}\tilde{G}_{rl}\tilde{f}_l(\omega). \quad \text{(B-3)}$$

This defines the amplitude coefficients in terms of f_i.

These amplitude coefficients can be substituted now in the total field of the half-space as given in equation A-4. Using equation 11 in the main text the Green's functions can be recognized. First, the $\tilde{\Gamma}_{33}^H$ as occurring in equation 24 is

$$\tilde{\Gamma}_{33}^H(p_1, p_2, z) = \tilde{\gamma}_3^H(p, z); \quad \text{(B-4)}$$

where $\tilde{\gamma}_3^H$ is given by

$$\begin{aligned}\tilde{\gamma}_3^H = &\frac{1}{2\rho}q_P\exp(i\omega q_P(z-h_2)) + \frac{p^2}{2\rho q_S}\exp(i\omega q_S(z-h_2))\\ &+\frac{1}{2\rho}[-q_P\tilde{R}_{PP}\exp(-i\omega q_P(z+h_2))\\ &+p\tilde{R}_{SP}\exp(-i\omega(q_S z + q_P h_2))]\\ &+\frac{p}{2\rho q_S}[q_P\tilde{R}_{PS}\exp(-i\omega(q_P z + q_S h_2))\\ &-p\tilde{R}_{SS}\exp(-i\omega q_S(z+h_2))]. \quad \text{(B-5)}\end{aligned}$$

Next, the values of $\tilde{G}_{3q3}^H$ are determined from $\tilde{\Gamma}_{33}^H$ via the deformation equation 4 and its equivalent $(\mathbf{p}, \omega)$-domain expression. Then the following expressions are obtained:

$$\tilde{G}_{313}^H(p_1, p_2, z) = \frac{p_1}{p}\tilde{g}_1^H(p, z), \quad \text{(B-6)}$$

$$\tilde{G}^H_{323}(p_1, p_2, z) = \frac{p_2}{p}\tilde{g}^H_1(p, z), \tag{B-7}$$

where $\tilde{g}^H_1$ is given by

$$\begin{aligned}\tilde{g}^H_1 = \frac{c_S^2}{2}&[-2pq_P \exp(i\omega q_P z) + 2pq_P \tilde{R}_{PP} \exp(-i\omega q_P z)\\ &+ (q_S^2 - p^2)\tilde{R}_{SP} \exp(-i\omega q_S z)] \exp(-i\omega q_P h_2)\\ &+ \frac{c_S^2}{2}\frac{p}{q_S}[(q_S^2 - p^2)\exp(i\omega q_S z)\\ &- 2pq_P \tilde{R}_{PS} \exp(-i\omega q_P z)\\ &- (q_S^2 - p^2)\tilde{R}_{SS} \exp(-i\omega q_S z)] \exp(-i\omega q_S h_2).\end{aligned} \tag{B-8}$$

and

$$\tilde{G}^H_{333}(p_1, p_2, z) = \tfrac{1}{2} + \tilde{g}^H_3(p, z). \tag{B-9}$$

The value $\tilde{g}^H_3$ is given by

$$\begin{aligned}\tilde{g}^H_3 = &-\frac{1}{2} + \left(\frac{1}{2} - p^2 c_S^2\right)\\ &\times \exp(i\omega q_P(z - h_2)) + c_S^2 p^2 \exp(i\omega q_S(z - h_2))\\ &+ \left(\frac{1}{2} - p^2 c_S^2\right)\tilde{R}_{PP} \exp(-i\omega q_P(z + h_2))\\ &- c_S^2 pq_S \tilde{R}_{SP} \exp(-i\omega(q_S z + q_P h_2))\\ &- \frac{p}{q_S}\left(\frac{1}{2} - p^2 c_S^2\right)\tilde{R}_{PS}\\ &\times \exp(-i\omega(q_P z + q_S h_2))\\ &+ c_S^2 p^2 \tilde{R}_{SS} \exp(-i\omega q_S(z + h_2)).\end{aligned} \tag{B-10}$$

In the calculations, the expressions of the Green's functions are needed in the $(\mathbf{x}, \omega)$ domain, so the above expressions need to be transformed back. For any Green's function $\tilde{G}$ in the $(\mathbf{p}, \omega)$ domain, the inverse transform is

$$\begin{aligned}\hat{G}(x, y) = \left(\frac{\omega}{2\pi}\right)^2 &\int_{-\infty}^{+\infty}\int_{-\infty}^{+\infty} \tilde{G}(p_1, p_2)\\ &\times \exp(-i\omega p_1 x - i\omega p_2 y)dp_1 dp_2.\end{aligned} \tag{B-11}$$

It is more convenient to go over to polar coordinates in p_1 and p_2 and also to introduce the polar coordinates for x and y via

$$p_1 = p\cos\phi \quad x = r\cos\psi$$

$$p_2 = p\sin\phi \quad y = r\sin\psi$$

Then the inverse transformation becomes

$$\begin{aligned}\hat{G}'(r, \psi) = \left(\frac{\omega}{2\pi}\right)^2 &\int_0^{+\infty}\int_0^{2\pi} \tilde{G}'(p, \phi)\\ &\times \exp[-i\omega pr\cos(\phi - \psi)]pd\phi dp.\end{aligned} \tag{B-12}$$

In this expression the Green's function $\tilde{G}$ is now written in terms of p and ϕ. For all of the Green's functions given in equations B4–B10, the integration suited for the cylindrical nature of the problem can be performed.

REFERENCES

Aki, K., and P. G. Richards, 1980, Quantitative seismology: Theory and methods: W. H. Freeman & Company.

de Hoop, A. T., 1995, Handbook of radiation and scattering of waves: Academic Press.

de Hoop, A. T., and J. H. M. T. Van der Hijden, 1985, Seismic waves generated by an impulsive point source in a solid/fluid configuration with a plane boundary: Geophysics, **50**, 1083–1090.

Drijkoningen, G. G., 2000, The usefulness of geophone ground coupling experiments to seismic data: Geophysics, **65**, 1780–1787.

Hoover, G. M., and J. T. O'Brien, 1980, The influence of the planted geophone on seismic land data: Geophysics, **45**, 1239–1253.

Krohn, C. E., 1984, Geophone ground coupling: Geophysics, **49**, 722–731.

Lamer, A., 1970, Couplage sol-geophone: Geophysical Prospecting, **18**, 300–319.

Tan, T. H., 1987, Reciprocity theorem applied to the geophone-ground coupling problem: Geophysics, **52**, 1715–1717.

Vos, J., G. G. Drijkoningen, and J. T. Fokkema, 1999, Sensor coupling in acoustic media using reciprocity: Journal of the Acoustic Society of America, **105**, 2252–2260.